OPEN

Ag nanoprisms with Ag$_2$S attachment

Shenglin Xiong[1,2], Baojuan Xi[1], Kang Zhang[1], Yifei Chen[1], Jianwen Jiang[1], Jiangyong Hu[3] & Hua Chun Zeng[1,4]

[1]Department of Chemical and Biomolecular Engineering, Faculty of Engineering, National University of Singapore, 10 Kent Ridge Crescent, Singapore 119260, [2]Key Laboratory of the Colloid and Interface Chemistry (Shandong University), Ministry of Education, and School of Chemistry and Chemical Engineering, Shandong University, Jinan, 250100, P. R. China, [3]Department of Civil and Environmental Engineering, Faculty of Engineering, National University of Singapore, 10 Kent Ridge Crescent, Singapore 119260, [4]Institute of Materials Research and Engineering (IMRE), 3 Research Link, Singapore 117602.

Triangular Ag nanoprisms are a type of most-studied noble-metal nanostructures over the past decade owing to their special structural architecture and outstanding optical and catalytic properties for a wide range of applications. Nevertheless, in contrast to active research for the synthesis of phase-pure Ag nanoprisms, no asymmetric heterodimers containing Ag prisms have been developed so far, probably due to lack of suitable synthetic methods. Herein, we devise a simple ion-exchange method to synthesize Ag$_2$S/Ag heterodimers at room temperature, through which Ag nanoprisms with controllable size and thickness can be fabricated. Formation chemistry and optical properties of the heterodimers have been investigated. These semiconductor/metal heterodimers have exhibited remarkable bactericidal activity to *E. coli* cells under visible light illumination.

I n addition to its well-known applications in ornaments, electrical conductors, mirrors, photographic films and antimicrobial[1–4], nanostructured silver (Ag) has undergone extensive investigation in recent years due to many promising applications of this noble metal in the fields of catalysis, electronics, optical labeling and biosensing[5–8]. In this regard, a great number of methods have been developed to generate nanoscale Ag crystals with different morphologies such as rod, wire, cube, platelet, decahedron, and bipyramid etc[9–23]. Among them, triangular Ag platelets (or "prisms") have received tremendous research attention over the past decade because they possess outstanding plasmonic features across both visible and IR regions; they also show significant surface-enhanced Raman signals, and can also be facilely functionalized with sulfur-containing adsorbates[17–20]. Concerning the synthesis of Ag prisms, two major approaches have been developed: photoinduced growth[17–21], and seed-mediated growth (or thermal process) in solution[22,23]. Using the photoinduced route, for example, the conversion from Ag sphere to triangular prism would not take place in the darkroom even for a period of more than 2 months[17], revealing that presence of photons is indispensable for the formation of Ag prisms.

The geometry and crystal orientation of such important Ag prisms have been well established[18,22]. As depicted in Figure 1a, for example, a rotation axis with 3-fold symmetry (C_3) is perpendicular to the largest surface planes of {111} of silver crystal. If they are attached with a secondary phase (*X*, for example, a semiconductor) on one of their three edges or corners, their overall symmetry will be significantly lowered (i.e., the point group is changed from D_{3h} to C_{2v}). By imposing this desymmetrization, one actually turns the Ag prisms into *X*/Ag heterodimers or binary nanocomposites. Furthermore, the newly added material phase *X* would likely alter the overall electronic structure and thus surface plasmonic resonance (SPR) feature of Ag prisms to some extent, resulting in novel properties that symmetric Ag prisms do not possess.

Regarding the preparation of general semiconductor/noble-metal heterodimers, significant advancements have been made in recent years[26–37]. Investigations on this type of materials include CdSe/Au[26–28], ZnO/Ag[29], ZnO/Au[30], CdS/Pt[31,32], PbS/Au[33,34], Ag$_2$S/Au[35], and Ag$_2$S/Ag as well[36–38]. Nevertheless, it should be mentioned that these semiconductor/noble-metal heterodimers all involve the growth of metals onto their semiconductor counterparts, and rather surprisingly, apart from sphere-like particles or polyhedrons, the metal phases have never been prepared into more anisotropic shape such as a triangular platelet structure. Furthermore, the size of metal phase seems always smaller than that of primary semiconductors, namely, noble metals in such reported heterodimers only serve as a secondary phase. It is our belief that by coupling a smaller semiconductor particle to a larger anisotropic metal crystal, new semiconductor/noble-metal heterodimers can be attained, that is, the metal now serves as a dominant material while the semiconductor as a secondary counterpart. Through this reverse structural transformation, additional functionalities of the metal crystals can be attained.
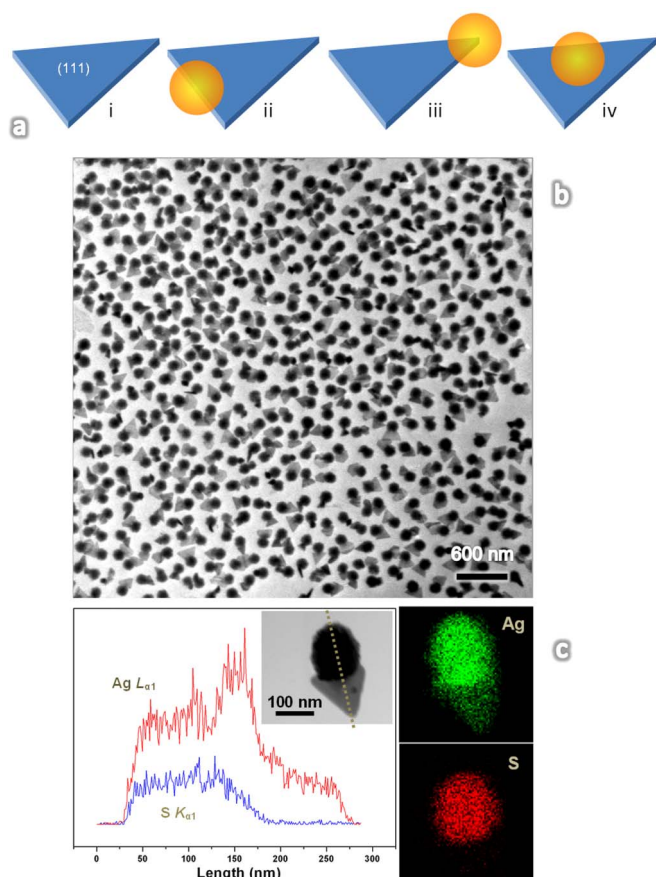
Figure 1 | Synthesis and characterization of Ag₂S/Ag heterodimers.
(a). Illustration of desymmetrization of Ag prism (in blue): (i) symmetric triangle, (ii) edge attachment, (iii) corner attachment, and (iv) planar attachment with an Ag₂S sphere (yellow), (b). a panoramic view (TEM image) of typical Ag₂S/Ag heterodimers (Experimental Section), and (c). TEM image, elemental line-profiles and chemical mappings of an Ag₂S/Ag heterodimer.

Very recently, we have synthesized Ag_2S/Ag heterodimers using a photoassisted solution-based approach[37]. Because the Ag crystal shape is sphere-like, the findings in that work could not be correlated directly to the rich literature reports for prismatic triangular silver. It should be mentioned that metallic or ionic Ag, which will be investigated in the present work, is a toxic element to microorganisms and shows prominent bactericidal activity against as many as 12 species of bacteria including *Escherichia coli*[24,25]. On the other hand, Ag_2S is both a direct narrow-band-gap semiconducting metal sulfide and an effective ionic semiconductor in which Ag^+ ions behave just like free electrons in metals resulting in cationic vacancy rich Ag_2S phase[39,40]. Such unique chemical and structural properties could endow it as an excellent host mediator for preparation of Ag_2S-based heterodimers with improved properties[36–38,42–45]. In addition to the connectivity to Ag, Ag_2S nanocrystals have also been demonstrated recently to act as a mediator/catalyst for preparation of semiconductor/semiconductor heterodimers such as Ag_2S/ZnS and Ag_2S/CdS in solution[41].

In this article, we have devised a convenient room temperature method for preparation of a new type of Ag_2S/Ag heterodimers without photon assistance. The following are the objectives of this work: (i) changing the silver phase to shape-defined Ag prisms, (ii) making the silver become a dominant phase in this binary heterodimers, and (iii) desymmetrizing Ag prisms in order to alter its surface plasmonic properties for new applications. While all these objectives have been achieved in the current study, our synthetic protocol also greatly simplifies the general preparation of triangular

Ag prisms at room temperature, because it does not need light irradiation, it does not require relatively strong reducing agent (e.g., L-ascorbic acid, $NaBH_4$, etc.), and it does not demand process heating (e.g., $\geq 60°C$) or use of seed in the previously reported methods[17,18,22]. These new Ag_2S/Ag heterodimers also exhibit significant enhancement in bactericidal ability for *E. coli* K-12 cells, compared to the Ag_2S/Ag in our earlier work[37]. The enhanced performance can be attributed largely to the realization of desymmetrizing triangular Ag prisms.

Results

We first synthesized monodisperse CdS colloidal nanospheres through a modified polyol process (Supplementary Information, SI-1). Transmission electron microscopy (TEM) images of the as-formed CdS nanospheres are displayed in Figure S1, which are at close to 100% morphological yield with an average diameter of 120 nm. Furthermore, our high-resolution TEM (HRTEM) investigation indicates that the nanospheres were formed through an oriented attachment mechanism with even smaller crystallites although there are structural defects due to rapid aggregation at high temperatures (Figure S2). The CdS nanospheres were used as a solid precursor for subsequent chemical transformation to Ag_2S nanospheres *via* cation-exchange and as a template for metallic Ag deposition. The resultant Ag_2S/Ag heterodimers from this process are depicted in Figure 1a.

In Figure 1b, the panoramic view on a product Ag_2S/Ag reveals that each Ag_2S nanosphere was grown with a triangular prism of Ag crystal, leading to formation of a novel type of asymmetric metal−semiconductor heterodimers. In this regard, the reported symmetrical nanoprisms of Ag have been desymmetrized for the first time due to attachment of Ag_2S phase. In general, the resultant Ag_2S/Ag heterodimers are also very uniform at a high morphological yield using this synthetic route (Figure 1b). It should be noted that the average diameter of the Ag_2S spheres in the dimers is around 120–130 nm, which is quite similar to that of the CdS precursor. From the high-magnification TEM image (Figure S3), we can find that the edge length of the Ag nanoprisms is about 200 nm, which is larger than the average diameter of Ag_2S. This type of heterodimers is structurally different from all other semiconductor−mental heterostructures reported in the literature[26–37]. Detailed characterization of these heterodimers is shown in Figure S3. Interestingly, the Ag platelets connect to Ag_2S nanospheres through a number of modes such as corner, edge, and face attachments (edge-attachment is dominant). Truncated Ag platelets could also be observed, though their population is low (Figure S3). In fact, all colloidal triangular nanoprisms/plates of silver reported in the literature always include certain percentages of non-triangular morphologies such as hexagons etc[19]. To confirm the resulted heterodimers, EDX line analysis and chemical mapping study were further conducted (Figure 1c). The $K_{\alpha 1}$ elemental line profiles distinctly show that sulfur element is distributed evenly in the Ag_2S solid spheres. A similar trend for the Ag $L_{\alpha 1}$ signal profile can also be observed for these nanospheres, noting that the drastic rise in signal at the juncture is a superimposition of Ag $L_{\alpha 1}$ signals arising from both Ag_2S and Ag phases. Therefore, the results revealed by the EDX analysis are in excellent agreement with those by the TEM. In addition, chemical mapping images of the Ag and S on the heterodimers further demonstrate the same elemental distributions (Figures S3 and S4). Ag nanoprisms could also be enlarged using the thus-grown Ag_2S/Ag as starting seeds. Such an epitaxial overgrowth is mainly an edge expansion of the Ag nanoprisms while their thickness is essentially unaltered (Figure S5). The image of Figure 2a shows a triangular Ag nanoprism prepared from the overgrowth of Ag. It exhibits sharp edges and corners, and smooth basal surfaces. The Ag_2S phase in this asymmetric heterodimer is a solid sphere. The electron diffraction (ED) pattern taken from the Ag nanoprism is composed of diffraction spots with a 6-fold rotational
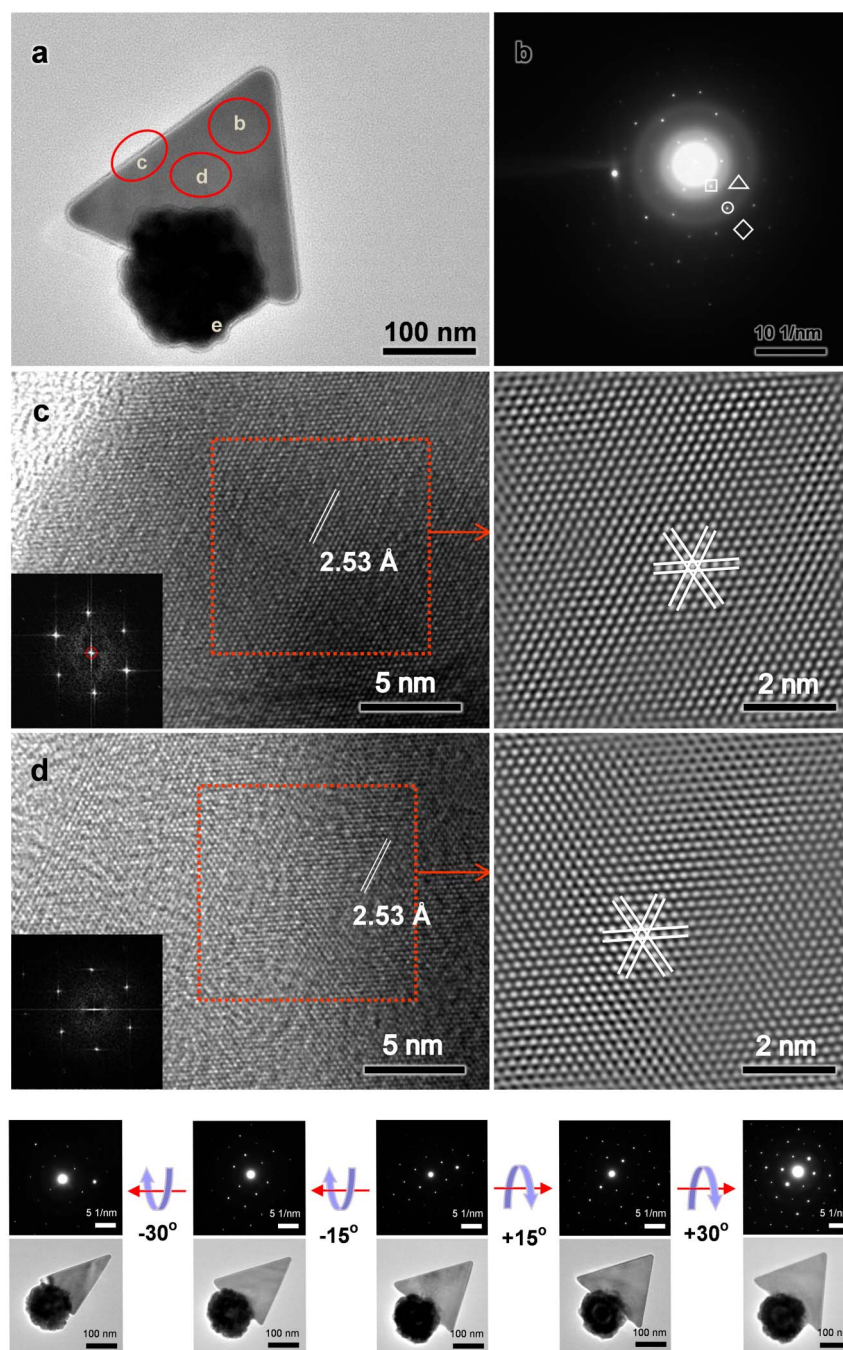
Figure 2 | TEM, SAED & HRTEM investigation of Ag₂S/Ag heterodimers. (a). TEM image of a representative Ag$_2$S/Ag heterodimer, (b). SAED pattern of (a)., where squared spots correspond to the formally forbidden 1/3{442} diffractions, triangle-framed spots to {202} diffractions, circled spots to 2/3{442} diffractions, and rhombic-shaped spots to {422} diffractions, and (c. & d.) HRTEM images and related FFT-images and ED patterns for the areas marked in (a).; details on the area (e of a.) can be found in Figure S6. TEM images (lower panel) and corresponding SAED patterns at various tilting angles.

symmetry (Figure 2b), revealing that the top and bottom faces of the Ag prism/plate are terminated by the {111} facets. Two sets of diffraction spots marked by square and circle with lattice facet spacing of 2.53 Å and 1.25 Å are corresponding to 1/3{-422} and 2/3{-422} respectively in accordance to previous reports[23], and the outer spot set (framed by a rhombus) is the diffractions of {-422} with an interplanar spacing of 0.835 Å. Another set of weak spots with a d-spacing of 1.46 Å can be identified as {220} diffraction normally allowed in fcc lattice. Figure 2c–d gives two HRTEM images taken along the [111] direction. The well-recognized lattice fringes further confirm the single crystal nature of the as-obtained Ag triangle plates, indexed

as the forbidden diffractions 1/3{-422} of fcc-lattice of Ag (also verified by Figure 2b). HRTEM images detected from different parts of a Ag$_2$S nanosphere have the clear lattice fringes with an interplanar spacing of approximately 0.26 nm, which is consistent well with the {-121} planes of the monoclinic Ag$_2$S, elucidating that these nanoparticles are single-crystalline (Figure S6).

The stereo-configuration of Ag$_2$S/Ag heterodimers is also examined in the TEM/SAED images of Figure 2 taken at different tilting angles. As reported in Figure S7, the thickness of nanoprisms increased only from ca 16 to 21 nm for the reaction times from 1 h to 5 days, while the edge-length of these nanoprisms increased

by more than 19 times from around 10 to 190 nm. This result shows that in the presence of polyvinylpyrrolidone (PVP), the Ag atoms were preferentially deposited on the side edges (i.e., {100}) of the triangular Ag instead of the {111} planes. To understand the role of this capping agent, we further carried out a molecular dynamic simulation (SI-2) for the adsorption of PVP on three common low Miller-indexed Ag surfaces. More detailed information on this simulation can be found in SI-2 and Figures S8 to S11. On the basis of this study, it is validated that PVP can bind more favorably to the {111} planes than to the {100} and {110} facets of Ag nanoprisms under our reaction conditions, consistent with the resultant Ag prism morphology reported in Figure 1 and Figure S3[16,22].

In order to understand the structural evolution of pristine CdS nanospheres to final Ag_2S/Ag heterodimers, X-ray diffraction (XRD) technique was also employed in this work. In Figure 3, a series of XRD patterns clearly confirms a gradual conversion of phase-pure hexagonal CdS (JCPDS card no. 41-1049; space group $P6_3mc$; lattice constants $a_o = 4.140$ Å and $c_o = 6.719$ Å) to the final Ag_2S/Ag composite (the monoclinic phase of Ag_2S: JCPDS card no. 14-0072, space group $P2_1/n$, lattice constants $a_o = 4.229$ Å, $b_o = 6.931$ Å, $c_o = 7.862$ Å, and $\beta = 99.61°$; and the fcc phase of Ag: JCPDS card no. 04-0783, space group $Fm\bar{3}m$, lattice constant $a_o = 4.086$ Å). In excellent agreement with the observed thin prism morphology, the (111) diffraction of the Ag phase is predominant. Accompanied with the phase evolution, EDX and XPS analyses further demonstrate that the solid spheres of CdS were converted essentially into Ag_2S/Ag heterodimers when the molar ratio of $AgNO_3$:CdS was set at 4 : 1 (Figures S12 & S13). The as-prepared Ag_2S/Ag heterodimers were also investigated with FTIR spectroscopy. As shown in Figure S14, Fourier transform infrared spectroscopy (FTIR) spectrum of the
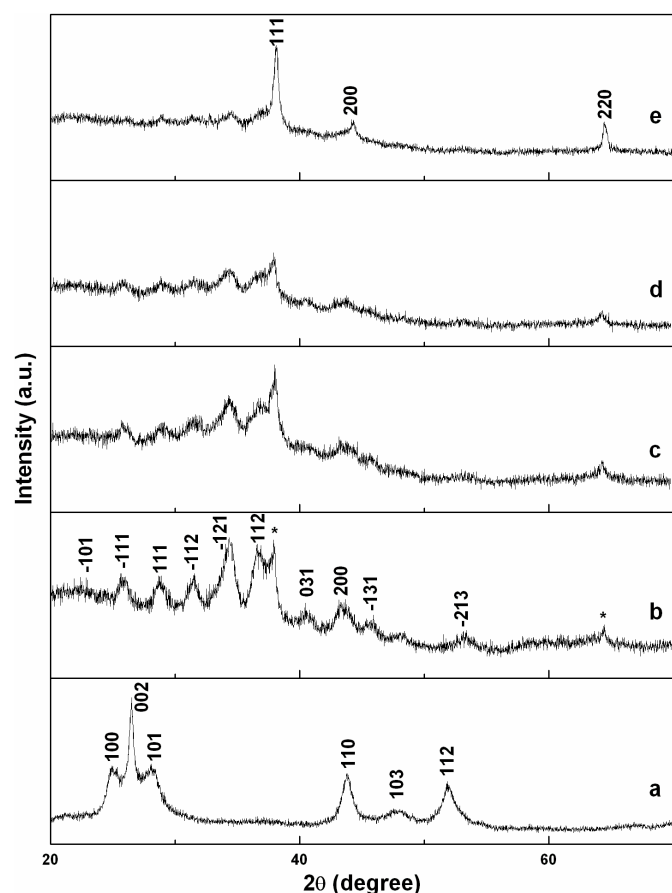
Ag_2S/Ag heterodimers is almost the same as that of pure PVP, showing several main absorption peaks located at 3444, 2956, and 1656 cm^{-1}, which can be assigned to the O–H, C–H, and C=O stretching modes respectively. It should be noted that the absorption peak of C=O bond at 1663 cm^{-1} for the pure PVP is shifted to 1656 cm^{-1} for the PVP on Ag_2S/Ag sample, which suggests a weak coordinative bonding of C=O (of PVP) to the surfaces of Ag nanoprisms. All these IR absorptions validate that the PVP macromolecules are anchored on the Ag_2S/Ag heterodimers. To further confirm this kind of interaction, a surface analysis with X-ray photoelectron spectroscopy (XPS) technique was also performed (Figure S15). Indeed, the study reveals electronic interactions between the Ag_2S/Ag and capping PVP, supporting the above FTIR findings.

As stated earlier, the molar ratio between $AgNO_3$ and CdS is a crucial parameter for the formation of Ag_2S/Ag heterodimers. When the $AgNO_3$:CdS ratio was smaller than 2 : 1, the Ag phase was largely in the form of sphere-like particles (Figure S16). If the $AgNO_3$:CdS was increased from 2 : 1 to 4 : 1, triangular Ag prisms became predominant in the product, and the size of Ag prisms increased from smaller than 50 to near 200 nm (Figure S16). This is understandable, because the newly formed Ag phase has located on the surface of Ag_2S upon the reduction by PVP; the prisms being formed can serve as favorable sites for continuous growth of silver. It is important to mention that only some irregular Ag particles could be generated in the absence of CdS solid precursor in the same reaction environment (EtOH-PVP), even with additional irradiation of UV-light (Figure S17). This indicates that the presence of Ag_2S is essential for the formation of Ag phase under this reaction setting. Our synthetic experiments show that the molar ratio of $AgNO_3$:CdS = 4 : 1 is an optimal condition for forming Ag_2S/Ag heterodimers with large Ag prisms yet without generating unattended Ag crystals. The presence of PVP is indispensable for forming Ag prisms (Figures S18 to S23). In this regard, we had also varied the quantity of PVP used in synthesis, and found that addition of 0.6 g of PVP is another optimal parameter to generate large Ag prisms (Figure S23).

To confirm the above reaction course, we further examined photon effect on the growth of Ag phase. Interestingly, similar Ag_2S/Ag products could be produced in the presence of either UV or visible light (Figures S24 to S27). Nevertheless, the conversion from CdS spheres to the Ag_2S/Ag heterodimers should be considered to be unrelated to the both kinds of light. In fact, the present formation reaction ($AgNO_3$ + CdS-EtOH-PVP) can be easily carried out at room temperature (25°C) without any light irradiation (i.e., under dark condition (SI-1), Figures S28 & S29), or strong reducing agent (e.g., L-ascorbic acid, $NaBH_4$, etc.), or addition of metal seeds. It is well-known that metallic Ag nanoparticles could be produced from $AgNO_3$ in the presence of ethanol and PVP or other nonionic surfactants[37,46–48]. In addition, our work indicates that $AgNO_3$ (dissolved in aqueous solution) can also react with CdS-PVP suspension in either aqueous or organic media (methanol, ethanol, 2-propanol, or ethylene-glycol) to generate Ag_2S/Ag heterodimers (Figures S30 to S31). The Ag_2S/Ag products can be easily stored as well. For example, the Ag_2S/Ag heterodimers are extremely stable in ethanol solvent at room temperature for a period of more than one year (Figure S32). As they are decorated with PVP, the heterodimers can be easily dispersed in polar solvents such as water or alcoholic organics.

Discussion

In our synthesis, the morphology of the Ag_2S/Ag was found to be dependent strongly on reaction parameters such as the process time, the molar ratio between $AgNO_3$ and CdS and the amount of PVP added. For instance, our time-dependent experiments in Figure 4 show that the addition of $AgNO_3$ into the starting CdS-EtOH-PVP suspension caused an immediate color change from yellow to gray, and then to black, indicating that such Ag_2S/Ag heterodimers were

Figure 3 | Structural characterization. XRD patterns of as-prepared CdS solid spheres (a). and Ag_2S/Ag heterodimers prepared with different mole ratios of $AgNO_3$:CdS [(b). 1:1, (c). 2:1, (d). 3:1, and (e). 4:1].

formed instantaneously. Due to an extremely small K_{sp} of Ag$_2$S (1.0 $\times$ 10^{-49}, 18°C), compared to that of CdS (8.0 $\times$ 10^{-27}, 18°C), the irreversible cation-exchange reaction between Cd^{2+} and Ag$^+$ takes place rapidly upon the addition of AgNO$_3$. Apart from the color change, the morphology of Ag phase evolves significantly upon the reaction time; it transforms from sphere-like nanoparticles to plate-like nanoparticles, and finally to triangular nanoprisms. The edge length of the attached Ag nanoprisms could be adjusted through controlling growth time (Figure 4). This product evolution is also reflected in the UV-visible-NIR absorption spectra displayed in Figure 5a. Similar to the previously reported results[42], all the spectra show a broad absorption band of Ag$_2$S centering around 497 nm. With extension of reaction time, these spectra gradually display three explicit peaks located at 342, 932, and 1040–1090 nm, respectively. Based on the previous studies[17,49,50], in particular, the first two peaks at shorter and mid wavelengths can be attributed to the out-of-plane and in-plane quadrupole excitations[23]; the red-shift in the latter could also arise from the existence of some truncated triangular prisms in the product[50]. The gradually increased peak in around 1040–1090 nm in NIR region could result from the in-plane dipolar excitation mode related with the prisms whose edge lengths exceeded 100 nm[18,23], which agrees well with the TEM observation of Figure 4. Importantly, the sharp peak at 1073 nm with a very narrow peak width observed in these Ag$_2$S/Ag heterodimers is an unprecedented phenomenon to the SPR investigations of phase-pure silver nano-structures, which may suggest an additional well-defined excitation

resonance resulting from effective coupling of this biphasic system at this wavelength.

To provide an in-depth insight to the change of SPR properties, the UV-visible-NIR absorption spectra have been simulated in this work using the dimensional data of the time-dependent TEM results (Figure 4). The average diameter of Ag$_2$S nanospheres used in the simulation was set at 125 nm, and the thickness of triangular Ag prisms was changed from 16 to 20 nm and the edge length was allowed to vary from 10 to 210 nm. In addition, truncation of the Ag prisms grown from 3 to 7 days was also taken into account. Figure 5b shows the simulated absorption spectra at different reaction times (Note: The time thereafter is actually correlated to dimensional data of the heterodimers). Initially at 1 h, a broad absorption peak at 340 nm (i.e., Ag$_2$S absorption) is observed. With increase in reaction time, three additional peaks appear at 500, 930, and 1070 nm, respectively. Quite encouragingly, these predicted peak positions are in accordance to those from the experimental measurements; even the sharp peak detected at 1073 nm (Figure 5a) is closely matched. The discrepancy in the peak shape and intensity at the NIR region can be attributed to multiple modes of attachment in the real samples, since we only performed the simulations for edge-attached heterodimers. Figure 6 gives the near-field images for the samples prepared at early reactions (1, 5, 10 and 18 h) plotted as intensity |E|. The incident light is perpendicular to the image plane, propagating in the x-axis and polarized in the z-axis. The wavelength of the incident light is based on the highest peak from the corresponding extinction
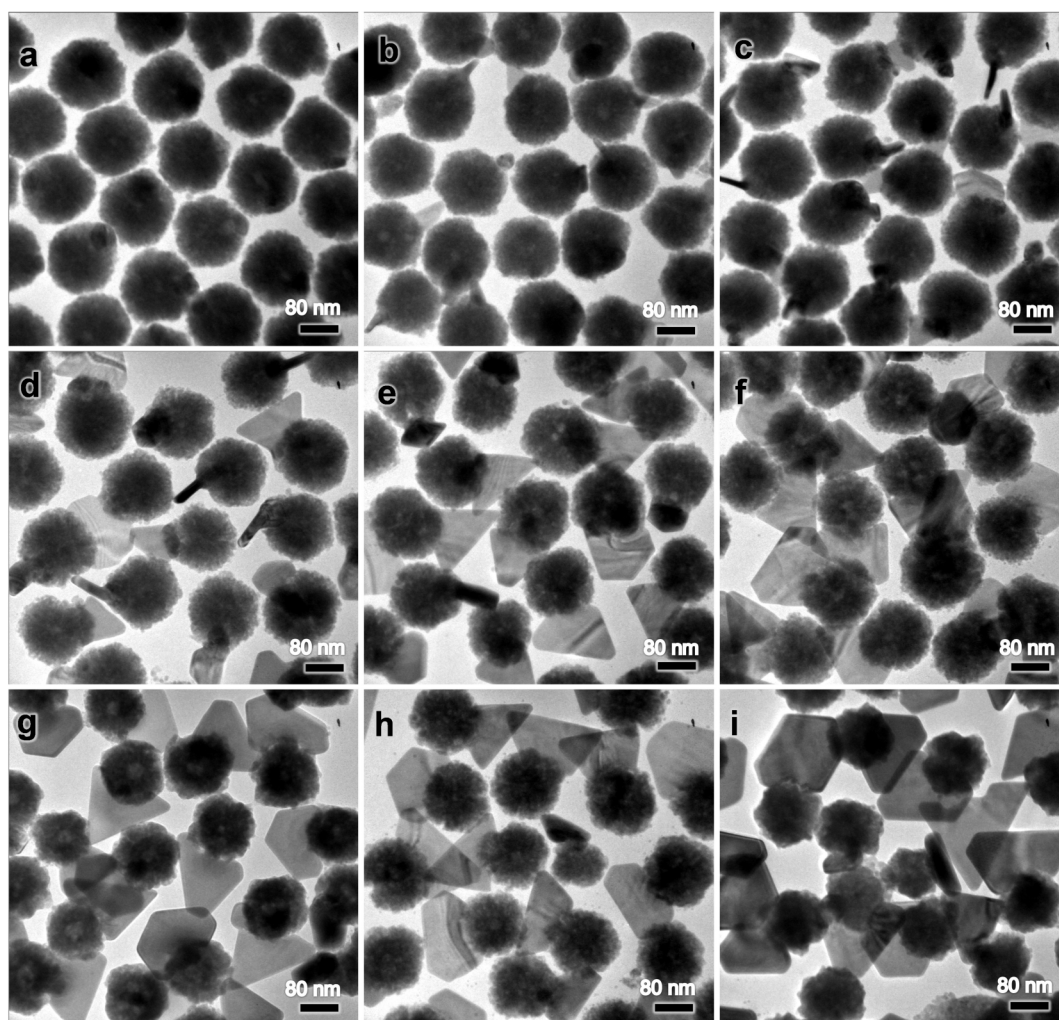
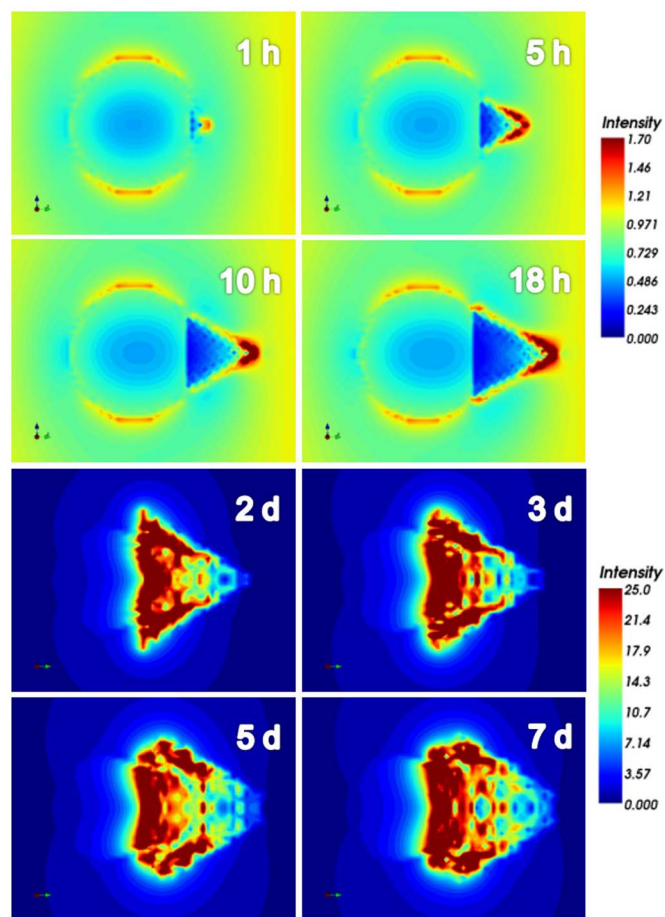**Figure 4 | TEM images of Ag$_2$S/Ag heterodimers.** The sample were prepared in the darkroom (Figures S28 & S29) at room temperature for different reaction times: (a). 1 h, (b). 5 h, (c). 10 h, (d). 18 h, (e). 2 days, (f). 3 days, (g). 4 d, (h). 5 days, and (i). 7 days.
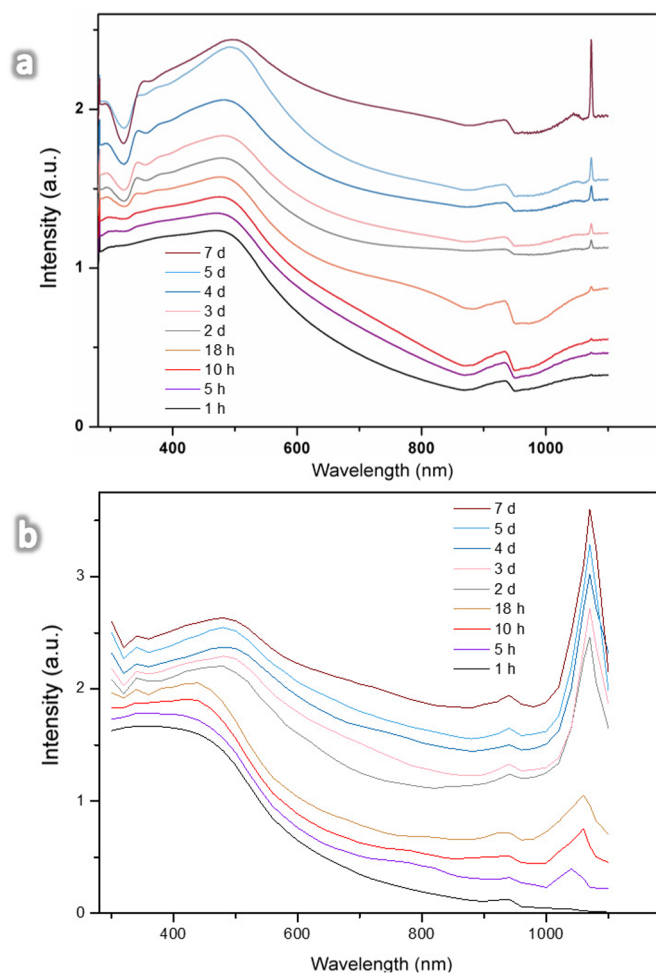
Figure 5 | Optical absorption properties. (a). Time-dependent UV-visible-NIR absorption spectra showing the evolution of Ag_2S/Ag in the dark at room temperature (i.e., the samples of Figure 4), and (b). Simulated absorption spectra of the samples in (a).

Figure 6 | Investigation on surface plasmonic resonance. Near-field images simulated for different edge-attached Ag_2S/Ag heterodimers at different growth times (refer to Figure 4, h = hour and d = day).

spectra (Figure S33). From 1 to 18 h (i.e., when Ag prisms are small), the Ag_2S sphere dominates the image and the lowest intensity is observed within the small triangular Ag prism. The image at 1 h is quite similar to that of a sphere[49], in which the two edges possess higher intensity. With increase in reaction time, the Ag prism starts to grow with increasingly stronger intensity on its tip, and significant near-field enhancement is observed on the extruding tip of the prism. The near-field enhancement for the larger Ag prisms (i.e., 2, 3, 5, and 7 days) is also very interesting. As shown in these images, the direction of incident light is the same for all the images, but the incident wavelength differs, since the highest peak of extinction curve shifts from 340 to 1070 nm (Figure S33). The observed red shift is primarily caused by the larger size of Ag prism in the latter samples. Comparing to the near-field image of 18 h sample, an enhancement for the sample grown after 2 days is observed on the two side-tips near the Ag_2S sphere (Figure 6)[50], noting that different incident wavelengths used in these simulations. Regarding the maximum intensity, there is also a substantial jump for the Ag prisms grown at 18 h to 2 days, increasing from 3.14 to 75.3. Such a near-field enhancement can also be augmented at the junction between two closely spaced particles. Therefore, the interface exhibits a higher intensity compared to normal triangular prism[49]. For all the samples grown during 2 to 7 days, there is no discernible near-field enhancement within the Ag_2S sphere. This further confirms that the small Ag_2S sphere has negligible contribution to the enhancement at long

wavelengths, but indeed it causes significant degeneracy in SPR properties due to desymmetrization of the Ag prisms. On the basis of these trial simulations, furthermore, one can now understand that the SPR properties depending on the size and location of Ag prisms when the size of Ag_2S sphere is fixed and the prepared heterodimers can be activated by the incident light across a wide span of photon wavelengths. Because the triangular Ag prisms in Ag_2S/Ag heterodimers have distinctive plasmonic enhancement modes for their two sets of tips (Figure 6) with different incident photons, this unique feature may enable these Ag_2S/Ag heterodimers for new applications.

To demonstrate this point further, we have used these samples for catalytic antibacterial application under either visible light exposure or darkroom condition (Experimental Section). In this set of tests, the photocatalytic ability of Ag_2S/Ag heterodimers for deactivation of *E. coli* was evaluated with a cell-concentration of about 1.0×10^8 CFU/mL, as reported in Figure 7. The reaction mixture containing *E. coli* cell suspension and the Ag_2S/Ag catalyst was placed under visible light for 0–40 min. As a reference, *E. coli* without Ag_2S/Ag was also irradiated for 50 min by UV light. Without catalysts, UV-light irradiation did not cause obvious bactericidal effects on *E. coli* (case a). However, the inactivation of *E. coli* was notably increased in the presence of our Ag_2S/Ag heterodimers under visible light, as compared to UV irradiation alone. The detected inactivation efficiencies were improved more than $5.0 \log_{10}$ units within 10 min and the *E. coli* cells could be largely deactivated within 20 min (case b) in the presence of only 0.01 mg/mL of Ag_2S/Ag heterodimers. The same amount of *E. coli* was completely killed within 5 min when the concentration of Ag_2S/Ag heterodimers was increased to 0.03 mg/mL
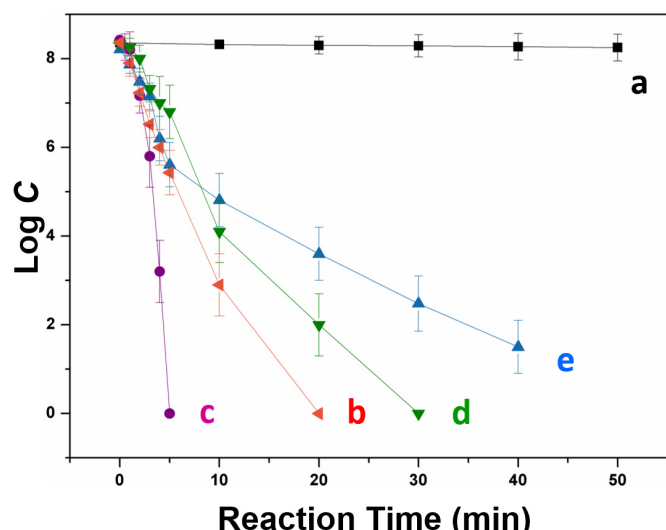
**Figure 7 | Inactivation efficiency against *E. coli* K-12.** (a). *E. coli* suspension without Ag$_2$S/Ag irradiated by UV light, (b). *E. coli* suspension with 0.01 mg/mL of Ag$_2$S/Ag heterodimers (prepared with standard conditions, Methods) under visible light, (c). *E. coli* suspension with 0.03 mg/mL of Ag$_2$S/Ag heterodimers (prepared with standard conditions, Methods) under visible light, (d). *E. coli* suspension with 0.01 mg/mL of Ag$_2$S/Ag in the dark condition, and (e). *E. coli* suspension with 0.01 mg/mL of Ag$_2$S/Ag with smaller triangular Ag prisms (edge-length 60–90 nm, Figure S30) under visible light.

under the same visible light exposure (case c); the curves within 5 min are detailed in Figure S34. The deactivation of *E. coli* was also evaluated in dark with the presence of Ag$_2$S/Ag heterodimers. Without light illumination (Figure 7d), however, the deactivation of *E. coli* is one or two orders in magnitude lower than that using the same amount of Ag$_2$S/Ag (0.01 mg/mL) but under the visible light. Nevertheless, the bacteria could also be completely inactivated at a longer reaction time (30 min, Figure 7d). In general, the inactivation efficiency is higher for larger Ag prisms, in comparison to that with smaller prisms (case e) (SI-1 & Figure S34). Under UV-light assistance, the synergetic effects of Ag$_2$S/Ag on bactericidal application have been explored in our previous work, where the Ag$_2$S is in a hollow sphere structure and the Ag is in an uncontrolled spherical shape in the studied heterodimers[37]. Without any light-assistance, in the present work, in contrast, it is surprising to see this new Ag$_2$S/Ag system with triangular Ag prisms can function much better in the same bactericidal application (Figure 7d). More importantly, it is clearly evidenced in Figure 7 that under the visible light, remarkable improvement in antimicrobial performance of Ag$_2$S/Ag heterodimers can be further attained.

To gain more understandings on the roles of the heterodimers in the above photocatalytic processes, the morphology of *E. coli* at different stages of bactericidal experiments in the presence of 0.01 mg/mL of Ag$_2$S/Ag was investigated by TEM and FESEM methods (Figures S35 & S36). Before light exposure (Figures S35 & S37), the ellipse-like *E. coli* bacteria held a well-defined cell wall and evenly distributed interior content. However, changes had taken place to the *E. coli* cells, when they were exposed to visible light for only 5 min (Figure S35); parts of cell membranes became disintegrated, suggesting that the decomposition of cells started from their membranes. Interestingly, it should be noted that Ag$_2$S/Ag heterodimers, especially the corners of Ag nanoprisms were bound to the outer membranes of the cell walls. Structurally, the tips of Ag prisms could behave like a "harpoon": once they contacted the surfaces of the cells, degradation of cell membrane would likely occur. Besides, the reaction system was well stirred, and the frequency of the collision

between the corners of Ag prisms and the cell walls must be high. In a certain sense, the Ag$_2$S/Ag heterodimers can function as effective antennas for different incident photons in view of their outstanding photo-absorbing ability (Figure 5) across UV-visible to NIR region. Furthermore, different sets of plasmonic "hot spots" at the corners of Ag prisms could be generated in accordance to the wavelengths of the absorbed photons (Figure 6). It is our belief that such intense localized electromagnetic fields are responsible for the observed cell membrane degradation. This finding is indicated more explicitly in Figure 8 for the *E. coli* cells with 10 min of light exposure; the outer walls largely disappeared and rumples/holes generated (Figure S35). With the time to 20 min, the outer cell walls disappeared completely and the amount of holes increased (Figure S35). On the contrary, the used Ag$_2$S/Ag heterodimers remained integral showing high structural stability under light irradiation. In order to exclude possible dissolution of Ag$^+$ ions from the above Ag$_2$S/Ag catalysts, we further used ICP-MS to determine the concentration of Ag$^+$ ions during the bactericidal processes. From Table S1 (SI-1), it can be seen that the Ag$^+$ concentration remained at an extremely low level of less than 2 ppm and did not change even after overnight reactions. EDX technique was also employed to determine the molar ratio of Ag:S for the spent catalysts. The measured molar ratio of Ag:S of the Ag$_2$S/Ag heterodimers after exposed by visible light for 30 min and placed with the *E. coli* cells overnight was 2.535, which was almost identical to the value (2.540) before their use (Table S1). On the basis of both ICP-MS/EDX results, it can be thus concluded that no net Ag$^+$ ions were released from the Ag$_2$S/Ag catalyst into the solution phase during the bactericidal processes.

In summary, this work is significant in the following aspects. First, it adds a new structural dimension and a semiconducting phase to the well-established triangular Ag nanoprisms, offering new research opportunity for investigating Ag-prism-containing nanocomposites. Second, it serves as a model example to bridge two important families of inorganic nanostructures (i.e., Ag nanoprisms and semiconductor/metal asymmetric heterodimers). And third, it demonstrates new possibility to employ the chemistry of cation-exchange, in combination
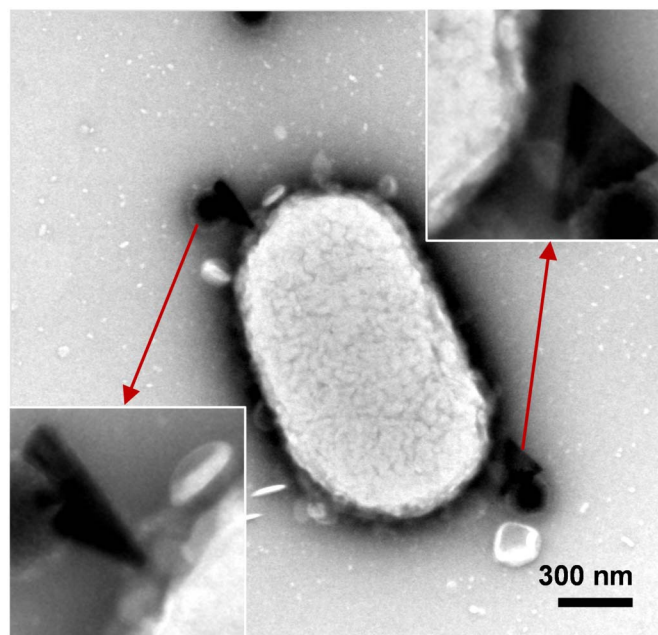
Figure 8 | TEM images of an *E. coli* cell together with two Ag$_2$S/Ag heterodimers. The test was carried out under visible light illumination for 10 min. Insets indicate the detailed views of the heterodimers. Note that the cell surface is decorated with sodium phosphotungstate (i.e., tiny crystallites scattered around the cell at lighter image contrast).

with redox reactions and with assistance of stabilizing agents, to prepare noble-metals into complex shapes for asymmetric heterostructures. As investigated above, this new type of photosensitive heterodimers may find future applications, including bacterial deactivation, bio-imaging and sensing, as well as heterogeneous catalysis under ambient conditions, by utilizing their synergistic properties of the biphasic architecture.

Methods

Chemicals. Cadmium nitrate (Cd(NO₃)₂·4H₂O, 99.5%, Merck), thiourea (TU, 99%, Merck), and silver nitrate (AgNO₃, AR@(ACS), Mallinckrodt Chemical), di(ethylene glycol) (DEG, 99%, Sigma-aldrich), polyvinylpyrrolidone (PVP K30, MW = 40,000), Fluka), sodium citrate dehydrate (Na₃CA·2H₂O, 99+%, Aldrich), ethanol (C₂H₅OH, absolute for analysis, ACS, Merck), acetone (C₃H₆O, HPLC, TEDIA). All reagents were used as received without further purification.

Synthesis of CdS colloidal nanospheres. The CdS colloidal nanospheres precursor was prepared through high-temperature polyol-mediated reaction. Briefly, 1.0 mmol of Cd(NO₃)₂·4H₂O, 0.83 g of PVP and 10 mL of DEG were poured into a three-necked flask. When the mixed solution was heated from room temperature to 160°C, 1.0 mmol of thiourea (TU, 99%)/DEG (2.0 mmol of TU) stock solution was injected rapidly into the hot solution. The solution turned to yellow when it reached 160 to 185°C (i.e., formation of CdS). The CdS suspension was kept at 185°C for 1 h. The product was rinsed 3 times by precipitation with a mixture of acetone and ethanol followed by centrifugation at 5900 rpm for 10 min and finally dispersed in ethanol or deionized water for further use.

Seed-free preparation of triangular Ag₂S/Ag heterodimers. In a typical synthesis, 0.2 mL of CdS suspension (0.05 M in ethanol, prepared above), 0.6 g of PVP, and 2 mL of ethanol were poured into a clean vial. The vial was then sealed by rubber septum and vigorously stirred for 20 min. After that, a given amount of AgNO₃ aqueous solution (0.4 mL, 0.10 M) was added dropwise into the above mixture and then stirred continually for 5 days in darkroom condition at 25°C; we used black plastic film to wrap the sample vials, and all the experiment steps were handled in the darkroom. After reaction, the black precipitate was harvested by centrifugation and washed with the mixture of acetone and ethanol more than 3 times and the sample was named as normal Ag₂S/Ag heterodimers. Some comparative experiments were also performed with identical synthetic procedures but under the irradiation of common white lamps or UV light. Unless otherwise specified, the molar ratio between AgNO₃ and CdS was set at 4 : 1 and the amount of PVP was 0.6 g.

Overgrowth of triangular Ag prisms. Based on the above description, initial Ag₂S/Ag heterodimers were prepared by reaction in dark condition for 4 days. The Ag₂S/Ag heterodimers then served as seeds, to which about 0.2 mL of 0.10 M AgNO₃ solution was added and stirred for another 2 days. The product was collected and washed using the same procedures described above.

Antibacterial tests with Ag₂S/Ag heterodimers. *E. coli* K-12 was cultured in a nutrient broth at 37°C overnight (i.e., 16–18 h) at 200 rpm in a rotary shaker to obtain the first generation cells. Then 1 mL of the first generation cultured suspension was taken out and transferred to another 30 mL of nutrient broth for another 4 h culture at 37°C in the same rotary shaker until reaching the log phase. Afterward, the *E. coli* cells were collected by centrifugation at 3500 rpm for 10 min, and the bacterial pellets were washed twice with sterilized Milli-Q water to remove residual culture media components. The as-prepared cells were then re-suspended and diluted to the required cell density of around 10⁸ colony-forming units per milliliter (CFU/mL) with sterilized Milli-Q water. 50 mL of *E. coli* suspension and a certain amount of the normal Ag₂S/Ag heterodimers (0.01 and 0.03 mg/mL, respectively) were added to a glass bottle. To ensure good mixing, the resultant suspension was magnetically stirred (set at 700 rpm) under light irradiation; a visible light lamp (30 W) at the ambient condition was used as a light source. The distance between the lamp and the reaction bottle was *ca.* 50 cm. Before and during the light exposure, a 0.50 mL aliquot of the reaction mixture was withdrawn at given time intervals and diluted serially with sterilized Milli-Q water to adjust the bacterial concentration to ensure the growing bacterial colonies could be counted accurately and easily. In this connection, 0.10 mL of the diluted mixture was spread on a nutrient agar medium, and the colonies were counted to determine the viable bacterial numbers after being incubated at 37°C for 18–24 h. All of the bactericidal experiments were carried out at room temperature and repeated no less than 5 to 10 times in order to ensure experimental accuracy; the measured data for each set of experiments were expressed with the mean and standard deviation. The diluted *E. coli* suspension without addition of the Ag₂S/Ag heterodimers was irradiated with a Philips HPR UV light source (a high pressure mercury lamp (125 W, the main emission wavelength: 365 nm (UV-A), and luminous efficacy: 23.2 lm/W) and a UV cutoff filter ($\lambda > 290$ nm), with other experimental conditions unchanged and was used as a control reference. In addition, culture experiments on the reaction mixture (i.e., *E. coli* together with normal Ag₂S/Ag heterodimers) in darkroom condition were also performed for comparison.

Details on the instrumental analysis and materials characterization for all the investigated samples in this work can be found in Supplementary Information (SI-1).

Simulation models and methods. Vinylpyrrolidone monomer was optimized using density functional theory (DFT)[51]. The atoms of PVP and Ag were mimicked by the COMPASS force field[52]. Molecular dynamics (MD) simulations were carried out in a canonical ensemble for three different types of systems, namely PVP chain, Ag surface and the complex with PVP adsorbed on Ag surface. The absorption spectra, extinction spectra, and surface plasmonic properties were simulated using discrete dipole approximation (DDA) as implemented in open source software namely DDSCAT[53]. The refractive index data of Ag and Ag₂S were adopted from the literature[54–56]. Further information on the simulations for PVP and Ag interactions can be found in Supplementary Information (SI-2).

1. Wiley, B. J. *et al.* Synthesis and electrical characterization of silver nanobeams. *Nano Lett.* **6**, 2273–2278 (2006).
2. Shen, L., Ji, J. & Shen, J. Silver mirror reaction as an approach to construct superhydrophobic surfaces with high reflectivity. *Langmuir* **24**, 9962–9965 (2008).
3. Rogach, A. L. *et al.* Changes in the morphology and optical absorption of colloidal silver reduced with formic acid in the polymer matrix under UV irradiation. *J. Phys. Chem. B* **101**, 8129–8132 (1997).
4. Kumar, A., Vemula, P. K., Ajayan, P. M. & John, G. Silver-nanoparticle-embedded antimicrobial paints based on vegetable oil. *Nat. Mater.* **7**, 236–241 (2008).
5. Henzie, J., Grünwald, M., Widmer-Cooper, A., Geissler, P. L. & Yang, P. Self-assembly of uniform polyhedral silver nanocrystals into densest packings and exotic superlattices. *Nat. Mater.* **11**, 131–137 (2012).
6. Wu, Y., Li, Y. & Ong, B. S. A simple and efficient approach to a printable silver conductor for printed electronics. *J. Am. Chem. Soc.* **129**, 1862–1863 (2007).
7. Schrand, A. M., Braydich-Stolle, L. K., Schlager, J. J., Dai, L. & Hussain, S. M. Can silver nanoparticles be useful as potential biological labels. *Nanotechnology* **19**, 235104 (2008).
8. Peng, H.-I., Strohsahl, C. M., Leach, K. E., Krauss, T. D. & Miller, B. L. Label-Free DNA Detection on Nanostructured Ag Surfaces. *ACS Nano* **3**, 2265–2273 (2009).
9. Pietrobon, B., McEachran, M. & Kitaev, V. Synthesis of Size-Controlled faceted pentagonal silver nanorods with tunable plasmonic properties and self-Assembly of these nanorods. *ACS Nano* **3**, 21–26 (2009).
10. Sun, Y. G., Gates, B., Mayers, B. & Xia, Y. N. Crystalline silver nanowires by soft solution processing. *Nano Lett.* **2**, 165–168 (2002).
11. Hu, J. Q. *et al.* A simple and effective route for the synthesis of crystalline silver nanorods and nanowires. *Adv. Funct. Mater.* **14**, 183–189 (2004).
12. Sun, Y. G. & Xia, Y. N. Shape-controlled synthesis of gold and silver nanoparticles. *Science* **298**, 2176–2179 (2002).
13. Zhang, Q. *et al.* Seed-mediated synthesis of Ag nanocubes with controllable edge lengths in the range of 30-200 nm and comparison of their optical properties. *J. Am. Chem. Soc.* **132**, 11372–11378 (2010).
14. Gao, Y. *et al.* Studies on silver nanodecahedrons synthesized by PVP-assisted N,N-dimethylformamide (DMF) reduction. *J. Cryst. Growth* **289**, 376–380 (2006).
15. Wiley, B. J., Xiong, Y. J., Li, Z.-Y., Yin, Y. D. & Xia, Y. N. Right bipyramids of silver: a new shape derived from single twinned seeds. *Nano Lett.* **6**, 765–768 (2006).
16. Zhang, J., Li, S. Z., Wu, J. S., Schatz, G. C. & Mirkin, C. A. Plasmon-mediated synthesis of silver triangular bipyramids. *Angew. Chem. Int. Ed.* **48**, 7787–7791 (2009).
17. Jin, R. C. *et al.* Photoinduced conversion of silver nanospheres to nanoprisms. *Science* **294**, 1901–1903 (2001).
18. Jin, R. C. *et al.* Controlling anisotropic nanoparticle growth through plasmon excitation. *Nature* **425**, 487–490 (2003).
19. Xue, C. & Mirkin, C. A. pH-switchable silver nanoprism growth pathways. *Angew. Chem. Int. Ed.* **46**, 2036–2038 (2007).
20. Xue, C., Métraux, G. S., Millstone, J. E. & Mirkin, C. A. Mechanistic study of photomediated triangular silver nanoprism growth. *J. Am. Chem. Soc.* **130**, 8337–8344 (2008).
21. Callegari, A., Tonti, D. & Chergui, M. Photochemically grown silver nanoparticles with wavelength-controlled size and shape. *Nano Lett.* **3**, 1565–1568 (2003).
22. Zeng, J. *et al.* Successive deposition of silver on silver nanoplates: lateral versus vertical growth. *Angew. Chem.* **123**, 258–263 (2011).
23. Sun, Y. G., Mayers, B. & Xia, Y. N. Transformation of silver nanospheres into nanobelts and triangular nanoplates through a thermal process. *Nano Lett.* **3**, 675–679 (2003).
24. Kim, J. S. *et al.* Antimicrobial effects of silver nanoparticles. *Nanomedicine* **3**, 95–101 (2007).
25. Zhao, G. J. & Stevens, S. E. Multiple parameters for the comprehensive evaluation of the susceptibility of *Escherichia coli* to the silver ion. *Biometals* **11**, 27–32 (1998).
26. Mokari, T., Rothenberg, E., Popov, I., Costi, R. & Banin, U. Selective growth of metal tips onto semiconductor quantum rods and tetrapods. *Science* **304**, 1787–1790 (2004).
27. Mokari, T., Sztrum, C. G., Salant, A., Rabani, E. & Banin, U. Formation of asymmetric one-sided metal-tipped semiconductor nanocrystal dots and rods. *Nat. Mater.* **4**, 855–863 (2005).
28. Zhao, N. N., Vickery, J., Guerin, G., Park, J., Winnik, M. A. & Kumacheva, E. Self-assembly of single-tip metal–semiconductor nanorods in selective solvents. *Angew. Chem. Int. Ed.* **50**, 4606–4610 (2011).

29. Pacholski, C., Kornowski, A. & Weller, H. Site-specific photodeposition of silver on ZnO ranorods. *Angew. Chem. Int. Ed.* **43**, 4774–4777 (2004).

30. Li, P., Wei, Z., Wu, T., Peng, Q. & Li, Y. D. Au-ZnO hybrid nanopyramids and their photocatalytic properties. *J. Am. Chem. Soc.* **133**, 5660–5663 (2011).

31. Dukovic, G., Merkle, M. G., Nelson, J. H., Hughes, S. M. & Alivisatos, A. P. Photodeposition of Pt on colloidal CdS and CdSe/CdS semiconductor nanostructures. *Adv. Mater.* **20**, 4306–4311 (2008).

32. Habas, S. E., Yang, P. & Mokari, T. Selective growth of metal and binary metal tips on CdS ranorods. *J. Am. Chem. Soc.* **130**, 3294–3295 (2008).

33. Shi, W. L. *et al.* A general approach to binary and ternary hybrid nanocrystals. *Nano Lett.* **6**, 875–881 (2006).

34. Yang, J., Elim, H. I., Zhang, Q., Lee, J. Y. & Ji, W. Rational synthesis, self-Assembly, and optical properties of PbS-Au heterogeneous nanostructures via preferential deposition. *J. Am. Chem. Soc.* **128**, 11921–11926 (2006).

35. Yang, J. & Ying, J. Y. Nanocomposites of Ag₂S and noble metals. *Angew. Chem. Int. Ed.* **50**, 4637–4643 (2011).

36. Yang, J., Sargent, E. H., Kelley, S. O. & Ying, J. Y. A general phase-transfer protocol for metal ions and its application in nanocrystal synthesis. *Nat. Mater.* **8**, 683–689 (2009).

37. Pang, M. L., Hu, J. Y. & Zeng, H. C. Synthesis, morphological control, and antibacterial properties of hollow/solid Ag₂S/Ag heterodimers. *J. Am. Chem. Soc.* **132**, 10771–10785 (2010).

38. Liu, B. & Ma, Z. F. Synthesis of Ag₂S–Ag nanoprisms and their use as DNA hybridization probes. *Small* **7**, 1587–1592 (2011).

39. Lim, W. P., Zhang, Z., Low, H. Y. & Chin, W. S. Preparation of Ag₂S nanocrystals of predictable shape and size. *Angew. Chem., Int. Ed.* **43**, 5685–5689 (2004).

40. Ivanov-Shitz, A. K. Computer simulation of superionic conductors: II. cationic conductors. review. *Crystallogr. Rep.* **52**, 302–315 (2007).

41. Zhu, G. X. & Xu, Z. Controllable growth of semiconductor heterostructures mediated by bifunctional Ag₂S nanocrystals as catalyst or source-host. *J. Am. Chem. Soc.* **133**, 148–157 (2011).

42. Kryukov, A. I., Stroyuk, A. L., Zin'chuk, N. N., Korzhak, A. V. & Kuchmii, S. Y. Optical and catalytic properties of Ag₂S nanoparticles. *J. Mol. Catal. A-Chem.* **221**, 209–221 (2004).

43. Motte, L. & Urban, J. Silver clusters on silver sulfide nanocrystals: synthesis and behavior after electron beam irradiation. *J. Phys. Chem. B* **109**, 21499–21501 (2005).

44. Terabe, K., Nakayama, T., Hasegawa, T. & Aono, M. Formation and disappearance of a nanoscale silver cluster realized by solid electrochemical reaction. *J. Appl. Phys.* **91**, 10110–10114 (2002).

45. Tang, Q. *et al.* Selective degradation of chemical bonds: from single-source molecular precursors to metallic Ag and semiconducting Ag₂S nanocrystals via instant thermal activation. *Langmuir* **22**, 2802–2805 (2006).

46. Ayyappan, S., Gopalan, R. S., Subbanna, G. N. & Rao, C. N. R. Nanoparticles of Ag, Au, Pd, and Cu produced by alcohol reduction of the salts. *J. Mater. Res.* **12**, 398 (1997).

47. Liz-Marzán, L. M. & Lado-Touriño, I. Reduction and stabilization of silver nanoparticles in ethanol by nonionic surfactants. *Langmuir* **12**, 3585–3589 (1996).

48. Wang, Y. *et al.* A convenient route to polyvinyl pyrrolidone/silver nanocomposite by electrospinning. *Nanotechnology* **17**, 3304–3307 (2006).

49. Hao, E., Schatz, G. C. & Hupp, J. T. Synthesis and optical properties of anisotropic metal nanoparticles. *J. Fluorescence* **14**, 331–341 (2004).

50. Zhao, L., Zou, S., Hao, E. & Schatz, G. C. Electrodynamics in computational chemistry. *Theor. Appl. Comput. Chem.* 47–65 (2005).

51. Materials Studio v. 4.3, Accelrys: San Diego (2007).

52. Sun, H. COMPASS: an *ab* initio force-field optimized for condensed-phase applications − overview with details on alkane and benzene compounds. *J. Phys. Chem. B* **102**, 7338–7364 (1998).

53. Draine, T. B. & Flatau, J. P. *User guide for the discrete dipole approximation code DDSCAT 7.2, 2012.*

54. Palik, E. D. *Handbook of optical constants of solids*, New York: Academic Press, pp. 350–357 (1985).

55. El-Nahass, M. M., Farag, A. A., Ibrahim, E. M. & Abd-El-Rahman, S. Structural, optical and electrical properties of thermally evaporated Ag₂S thin films. *Vacuum* **72**, 453–459 (2004).

56. Bennett, J. M., Stanford, J. L. & Ashley, E. J. Optical constants of silver sulfide tarnish films. *J. Optical Soc. Am.* **60**, 224–232 (1970).

Acknowledgements

Author contributions

S.L.X. and B.J.X. designed and performed the experiments. K.Z. and Y.F.C. carried out the computer simulations. H.C.Z., J.Y.H. and J.W.J. supervised the respective experiments and simulations. All authors contributed to the paper writing. H.C.Z. conceived the overall project and wrote the final manuscript.

Additional information

Supplementary information accompanies this paper at http://www.nature.com/scientificreports

Competing financial interests: The authors declare no competing financial interests.

How to cite this article: Xiong, S. *et al.* Ag nanoprisms with Ag₂S attachment. *Sci. Rep.* **3**, 2177; DOI:10.1038/srep02177 (2013).